Science Advances
AAAS

advances.sciencemag.org/cgi/content/full/4/8/eaas8772/DC1

Supplementary Materials for

Transparent and conductive nanomembranes with orthogonal silver nanowire arrays for skin-attachable loudspeakers and microphones

Saewon Kang, Seungse Cho, Ravi Shanker, Hochan Lee, Jonghwa Park, Doo-Seung Um, Youngoh Lee, Hyunhyub Ko*

*Corresponding author. Email: hyunhko@unist.ac.kr

Published 3 August 2018, *Sci. Adv.* **4**, eaas8772 (2018)
DOI: 10.1126/sciadv.aas8772

The PDF file includes:

Fig. S17. Waveform and STFT signals of original sound ("There's plenty of room at the bottom") extracted by the sound wave analyzer, where the signal was read from a commercial microphone.
Fig. S18. FFTs extracted from the sound wave of the word "nanomembrane" obtained from voices of different subjects including the registrant, the authorized user, and the denied user.
Fig. S19. FFTs extracted from the sound wave, obtained from the voice of a registrant.
Fig. S20. FFTs for a test repeated 10 times, extracted from the sound wave of the word "hello" obtained from various voices of different subjects including the registrant, a man, and two women.

Other Supplementary Material for this manuscript includes the following:

(available at advances.sciencemag.org/cgi/content/full/4/8/eaas8772/DC1)

Movie S1 (.mp4 format). Mechanical durability of hybrid NM.
Movie S2 (.mp4 format). Compression and stretching test of hybrid NM.
Movie S3 (.mp4 format). Skin-attachable NM loudspeaker.
Movie S4 (.mp4 format). The voice recognition using NM microphone.
Movie S5 (.mp4 format). Voice-based security system.

Supplementary Materials

Section S1. The calculated bending stiffness of the thin film

For the calculation of bending stiffness of hybrid nanomembranes, a representative cross-sectional geometry of the thin film is illustrated in fig. S4. In this structure, there are *n* AgNWs with a radius of *r* and Young's modulus of 83 GPa, which were wrapped by a parylene film with the size of $b \times h$ and Young's modulus of 3.2 GPa. The distance between the neutral axis and bottom of the thin film is

$$y_0 = \frac{h}{2} * \frac{1 + \frac{2h' + 2r}{h}\left(\frac{E_{\mathrm{Ag}}}{E_{\mathrm{Pa}}} - 1\right) n\pi r^2 \Big/ bh}{1 + \left(\frac{E_{\mathrm{Ag}}}{E_{\mathrm{Pa}}} - 1\right) n\pi r^2 / bh} \quad (1)$$

where y_0 is the distance between the neutral axis and bottom of the thin film, h is the thickness of film, h' is the distance between bottom of AgNWs and thin film, r is the radius of AgNWs, b is the width of parylene film, and E_{Ag} and E_{Pa} are the Young's modulus of silver and parylene, respectively. From the value of y_0, we can calculate the bending stiffness (*EI*) using the equation as below

$$EI = E_{\mathrm{Pa}} bh\left(\frac{1}{3}h^2 - hy_0 + y_0^2\right) + \left(E_{\mathrm{Ag}} - E_{\mathrm{Pa}}\right) n\pi r^2 \left[\frac{4}{3}r^2 + 2r\left(h' - y_0\right) + \left(h' - y_0\right)^2\right] \quad (2)$$

Section S2. The measured bending stiffness of the thin film

To investigate the measured bending stiffness of hybrid nanomembranes as a function of the density of orthogonal AgNW arrays, we assumed the hybrid NM as a single film and calculated the bending stiffness using the equation

$$EI = E_{Hybrid}\, bh\left(\frac{1}{3}h^2 - hy_0 + y_0^2\right) \tag{3}$$

Here, $\boldsymbol{E_{Hybrid}}$ is the Young's modulus of hybrid NM with orthogonal AgNW arrays, which was experimentally obtained from the capillary wrinkling test.

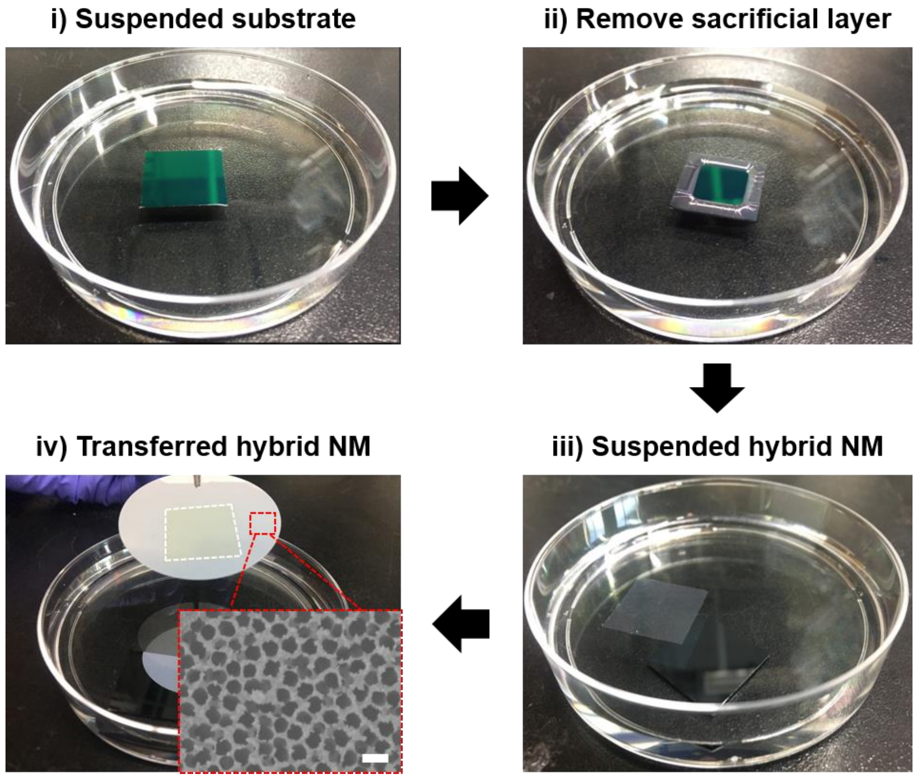

Fig. S1. Fabrication of the freestanding hybrid NM with the orthogonal AgNW array by removing the sacrificial layer. i) Floating of as-fabricated Si/ZnO/hybrid NM on an etchant solution. ii) Removing of a ZnO sacrificial layer. iii) Suspended hybrid NM on the etchant solution after etching process. iv) Transferred hybrid NM on an AAO template. Inset shows a SEM image of the AAO template. Scale bar in inset indicates 500 nm.

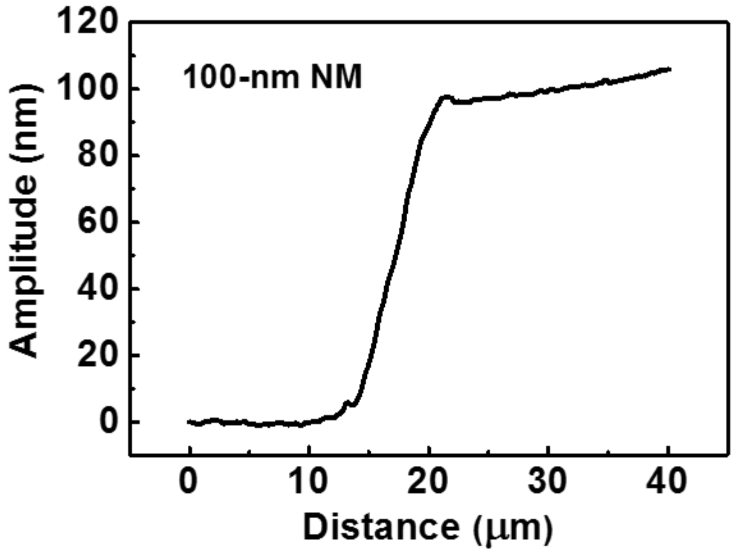

Fig. S2. Total thickness of the hybrid NM measured by atomic force microscopy.

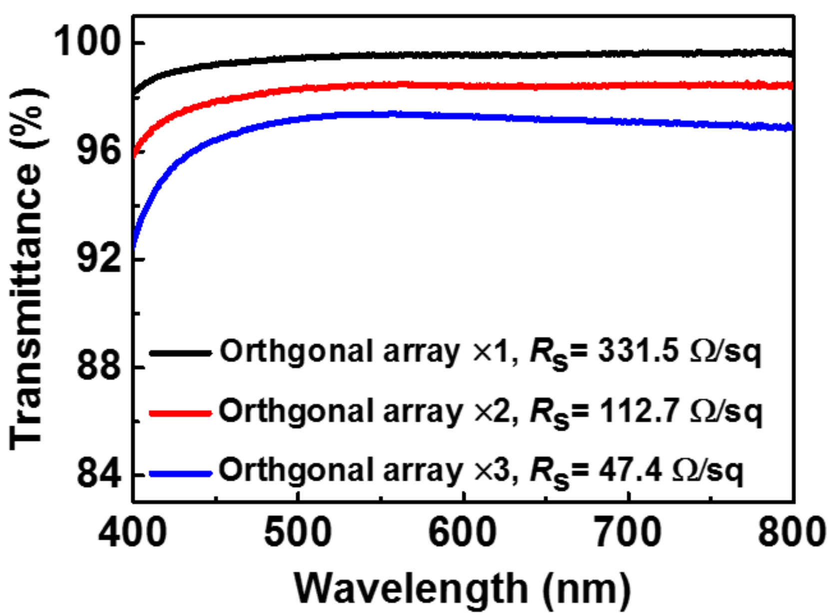

Fig. S3. Transmittance in the visible range of 400 to 800 nm and corresponding sheet resistance, R_s, of the orthogonal AgNW array with different numbers of orthogonal coatings.

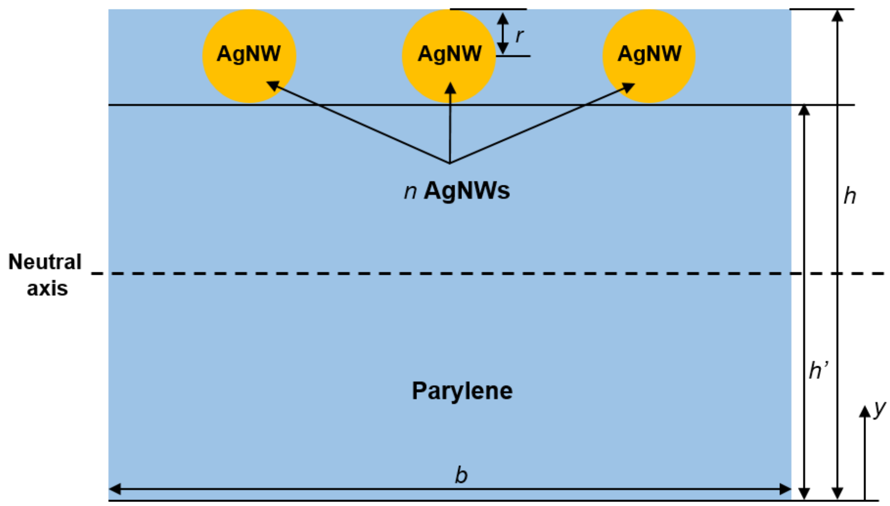

Fig. S4. The structural design of the hybrid NM for the calculation of the bending stiffness with geometrical parameters illustrated.

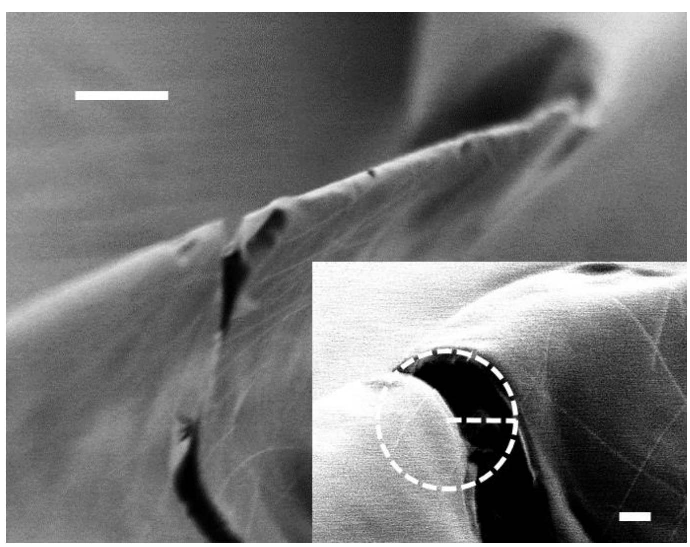

Fig. S5. SEM images of the hybrid NM folded in half. The scale bar indicates 5 μm. Inset shows enlarged SEM image of the folded hybrid NM with a bending radius of ~2.2 μm. The scale bar in inset indicates 1 μm.

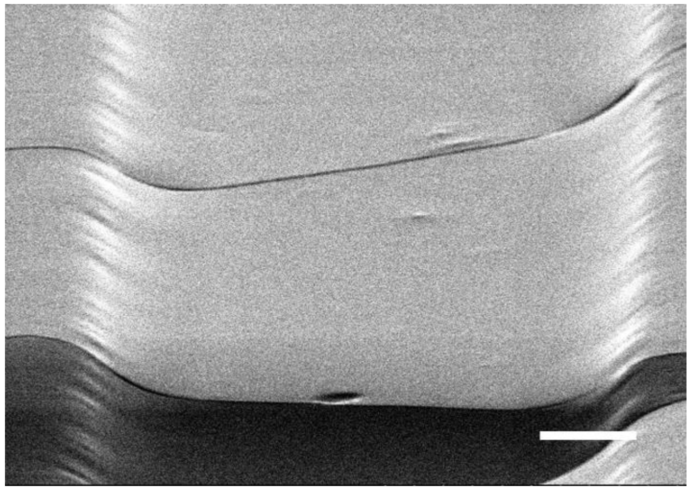

Fig. S6. High-magnitude SEM images of the hybrid NM transferred on the line-patterned PDMS with a line width of 20 µm. The transferred hybrid NM is intimately adhered to the surface of line patterns and even along the edges of the line patterns. The scale bar indicates 10 µm.

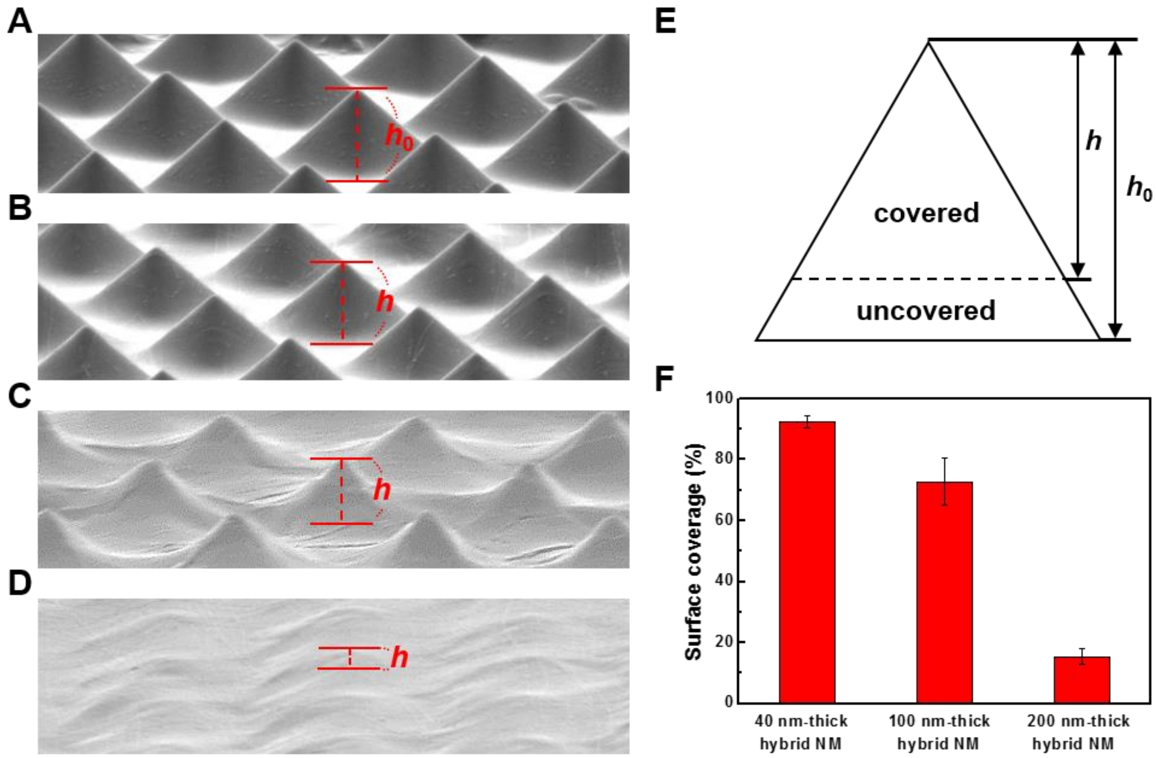

Fig. S7. Estimated step surface coverage of the hybrid NMs with different thickness placed on a micropyramid-patterned PDMS substrate. SEM images of (**A**) micropyramid-patterned PDMS substrate covered with (**B**) 40 nm-thick hybrid NM, (**C**) 100 nm-thick hybrid NM, and (**D**) 200 nm-thick hybrid NM. (**E**) Schematic diagram for the calculation of the step surface coverage (ratio of film-covered height to the total height of 3D structure) by comparing the height of triangles covered by hybrid NMs with different thickness. The step surface coverage can be estimated by $h/h_0 \times 100$ where h_0 is the height of micropyramid patterns and h_1 is the height that covered by hybrid NMs. (**F**) Estimated step surface coverage of the hybrid NMs with 40, 100, and 200 nm-thick hybrid NMs.

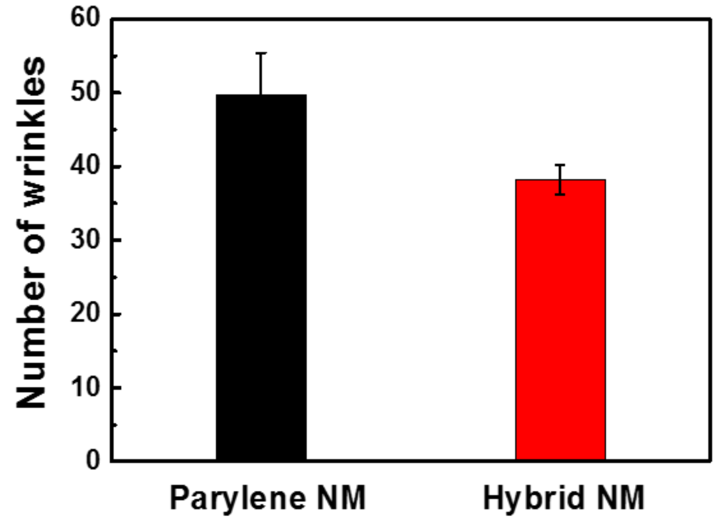

Fig. S8. Number of wrinkles generated from a pure parylene NM and hybrid NMs.

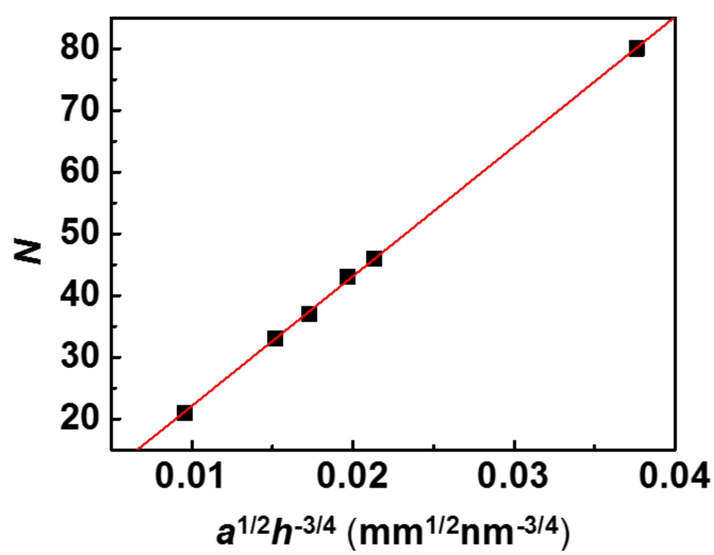

Fig. S9. Variation in the number of wrinkles N as a function of $N \sim a^{1/2}h^{-3/4}$.

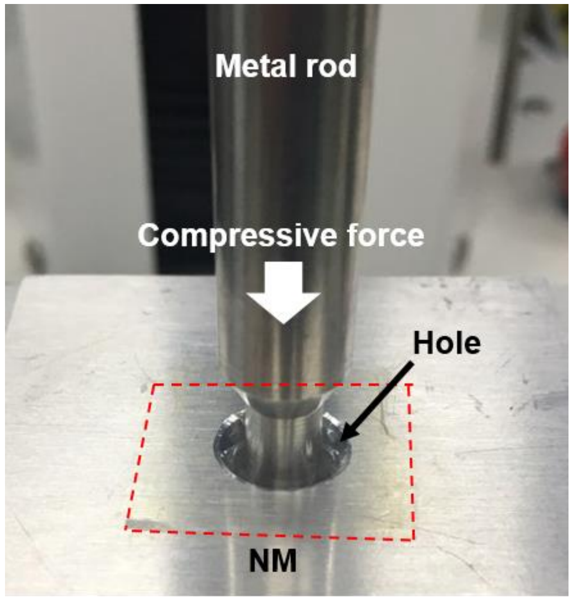

Fig. S10. Indentation test for measuring the mechanical properties of NMs. A metal rod applies a compressive force to the NMs mounted in the hole of the aluminum frame, descending at a constant velocity.

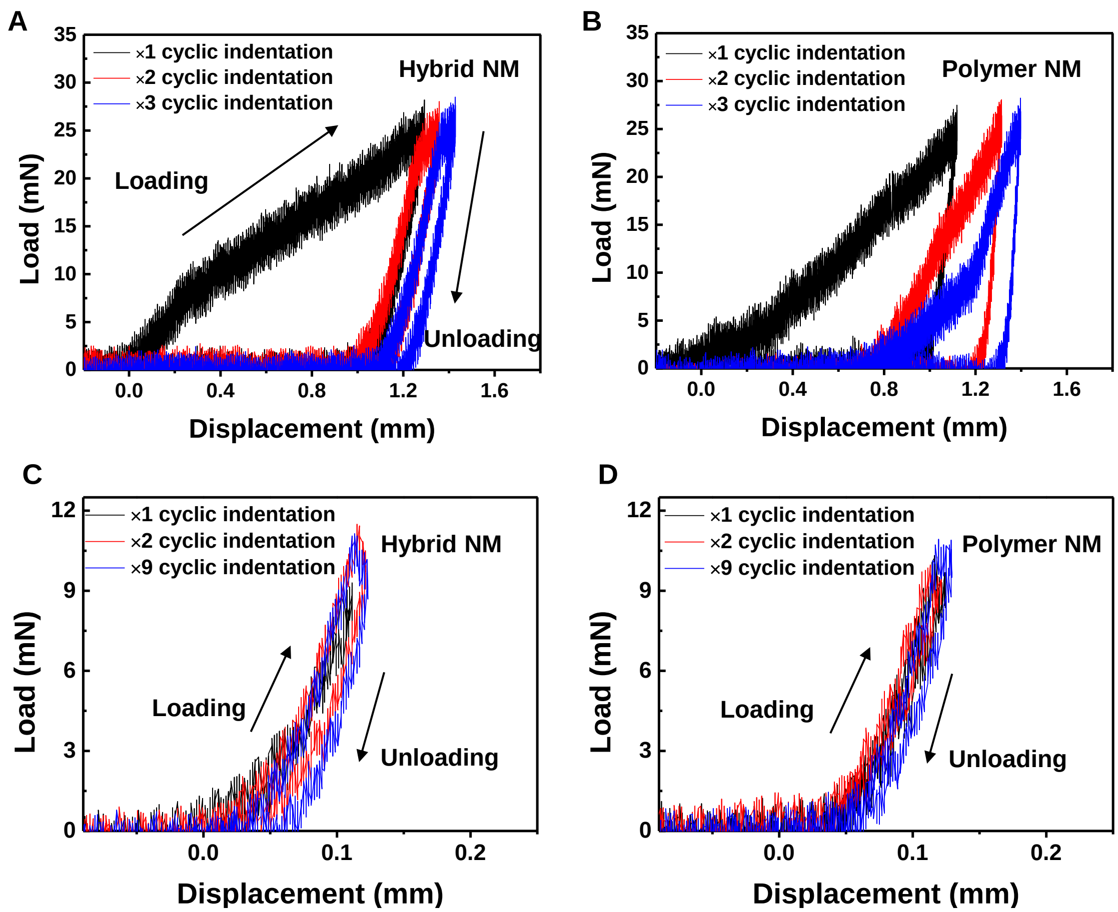

Fig. S11. Loading-unloading indentation test. Cyclic indentation load versus displacement curves of free-standing hybrid NM and polymer NM for an indentation load of (**A** and **B**) ~27 mN and (**C** and **D**) ~11 mN, respectively.

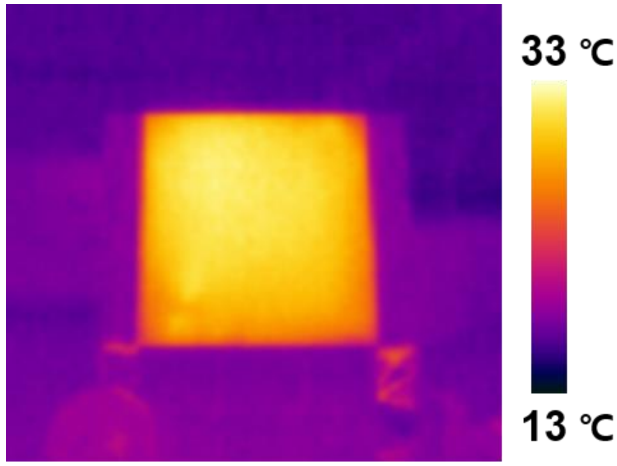

Fig. S12. IR images of the orthogonal AgNW array with AC 10 V applied at a frequency of 10 kHz.

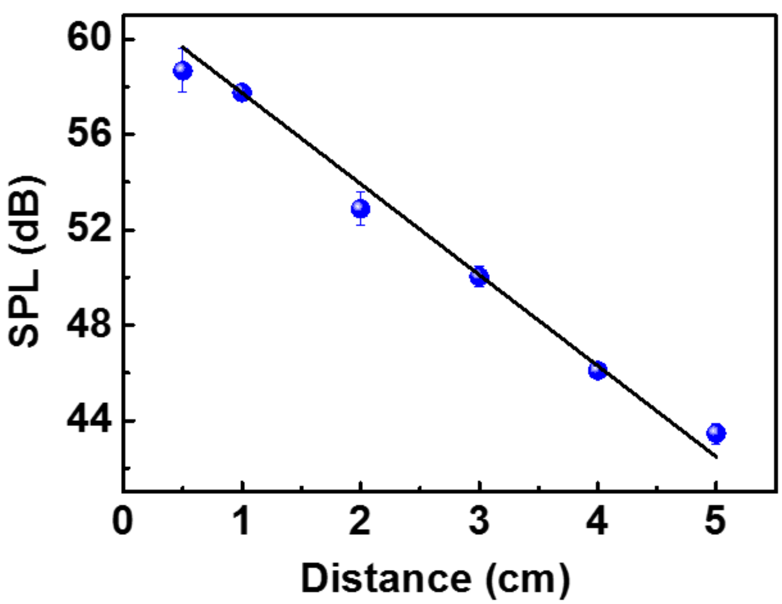

Fig. S13. SPL versus distance between the commercial microphone and the thick-film loudspeaker with the orthogonal AgNW array.

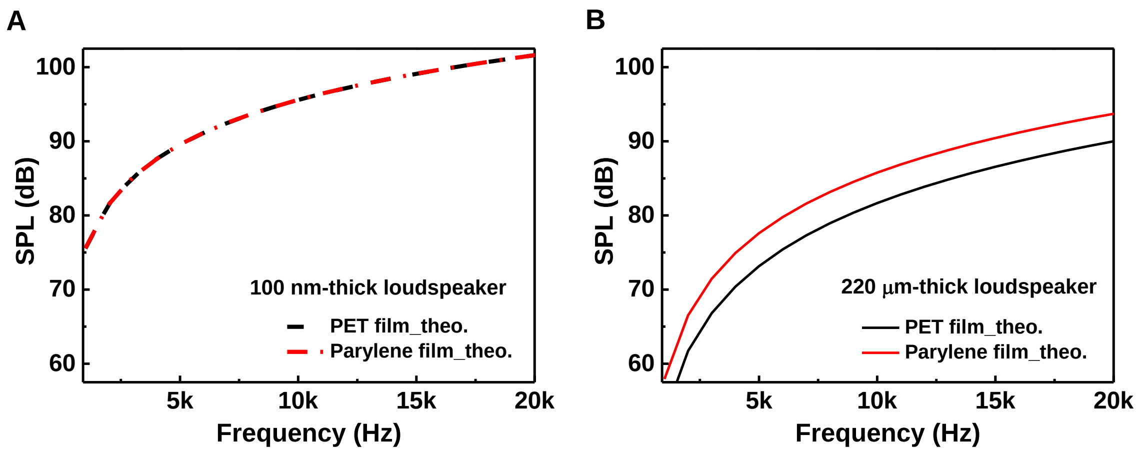

Fig. S14. Theoretical values of SPL as a function of sound frequency for loudspeakers with different thickness and substrates. (**A**) 100 nm-thick and (**B**) 220 μm-thick loudspeakers with different substrates.

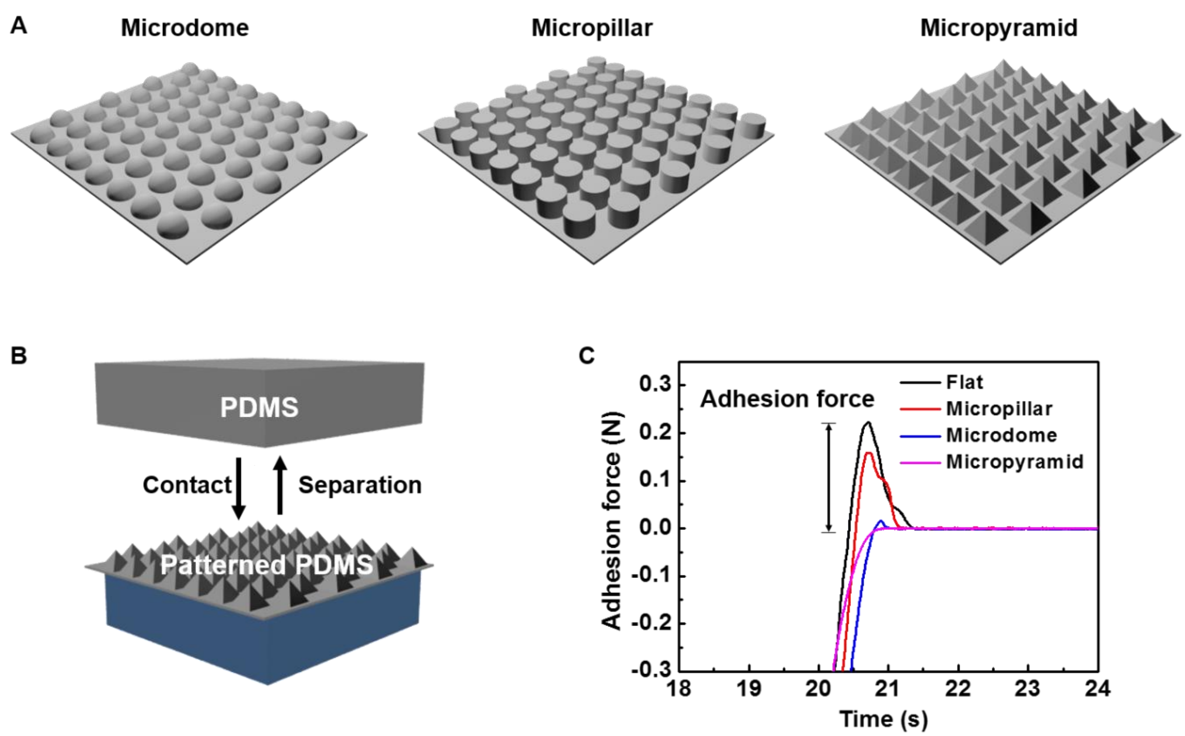

Fig. S15. Comparison of adhesion force of various micropatterned PDMS films. (**A**) Schematics of different micro-patterned (dome, pillar, and pyramid) PDMS films. (**B**) Schematic of system for measuring adhesion force between the micro-patterned PDMS and bare PDMS. (**C**) Adhesion force between the bare PDMS and different-patterned PDMS films.

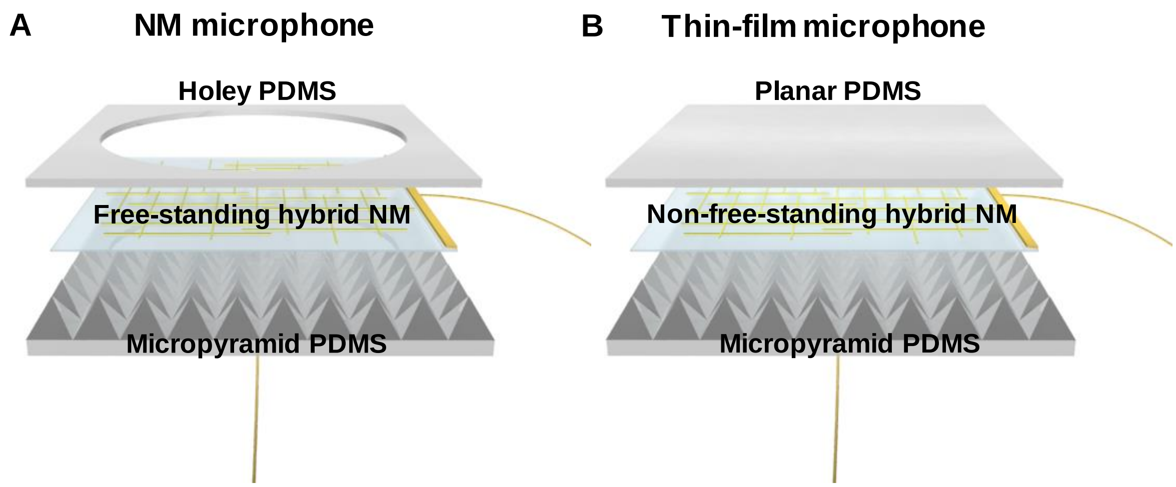

Fig. S16. Schematics showing the structure of microphone devices. (**A**) In the NM microphone, NMs are mounted to the “holey” PDMS film as a free-standing geometry. (**B**) In the thin-film microphone, a hybrid NM mounted to a planar PDMS film without a hole is fully laminated with the surface of PDMS film, where NMs cannot be free-standing.

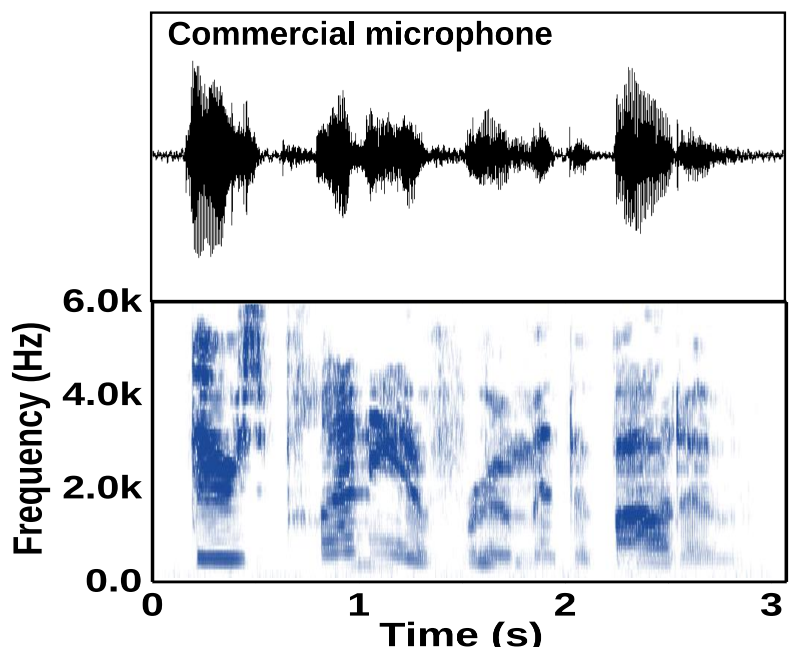

Fig. S17. Waveform and STFT signals of original sound (“There’s plenty of room at the bottom”) extracted by the sound wave analyzer, where the signal was read from a commercial microphone.

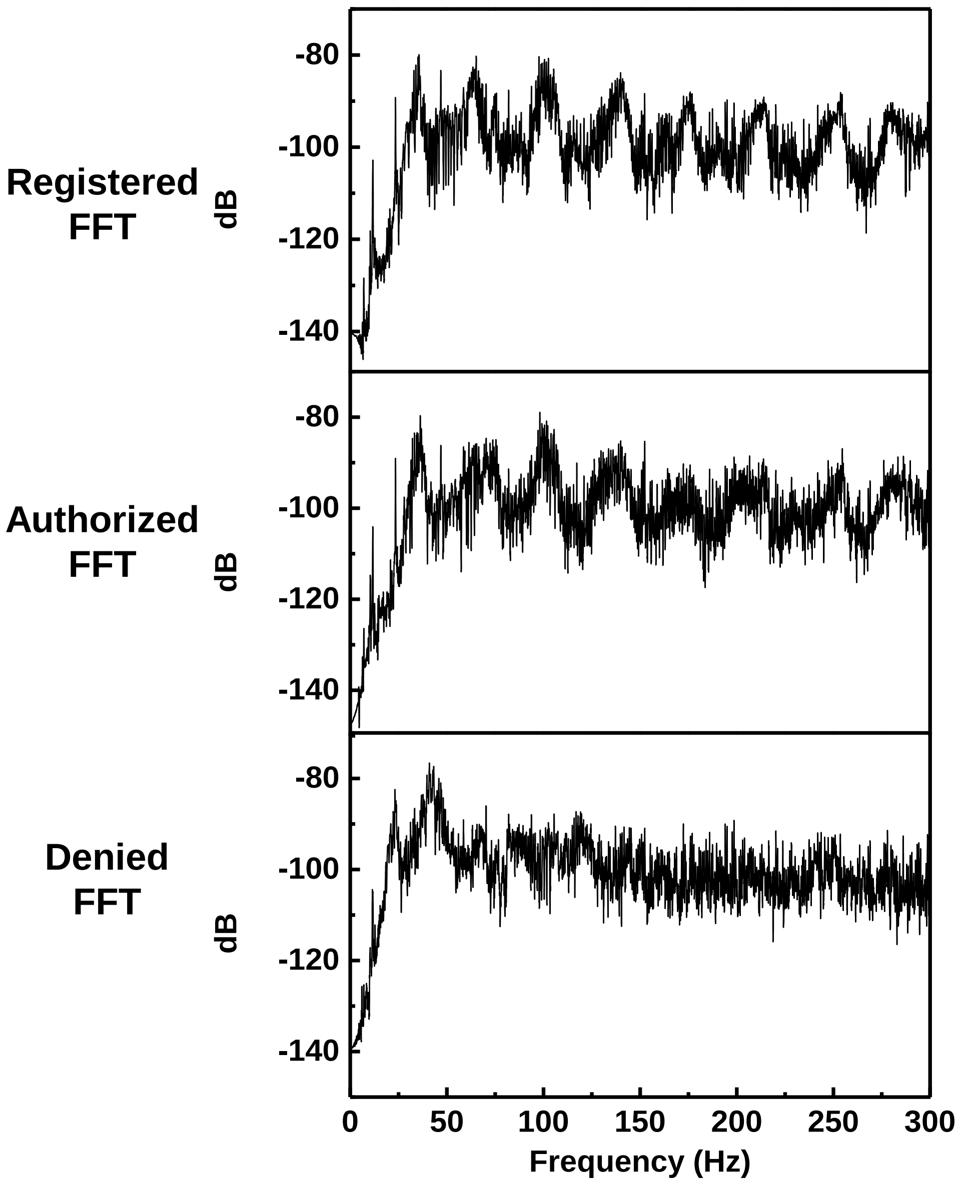

Fig. S18. FFTs extracted from the sound wave of the word "nanomembrane" obtained from voices of different subjects including the registrant, the authorized user, and the denied user.

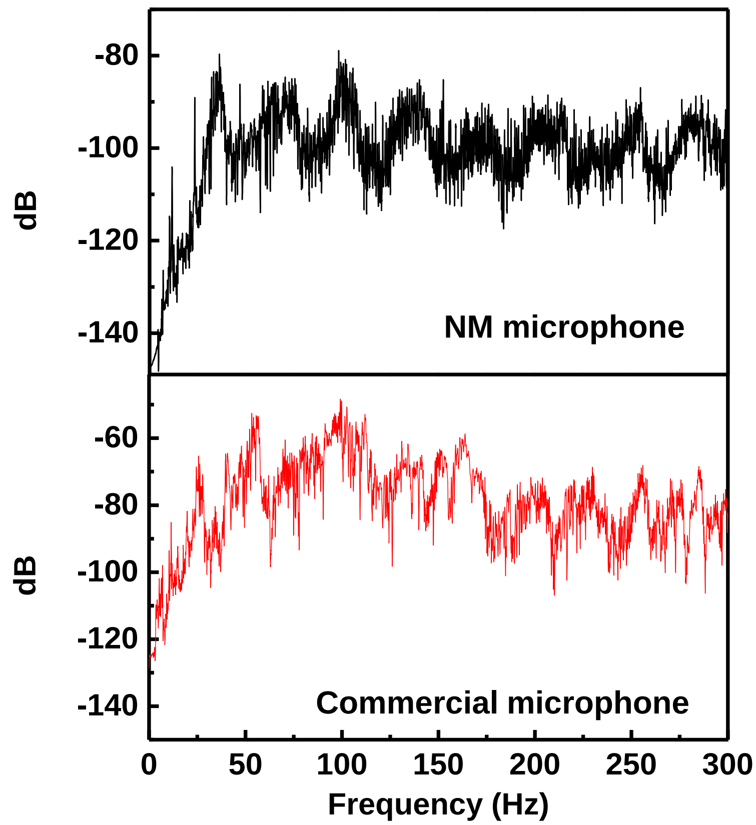

Fig. S19. FFTs extracted from the sound wave, obtained from the voice of a registrant. (upper) FFTs recorded using NM microphone and (bottom) FFTs recorded using commercial microphone (40PH, G.R.A.S.).

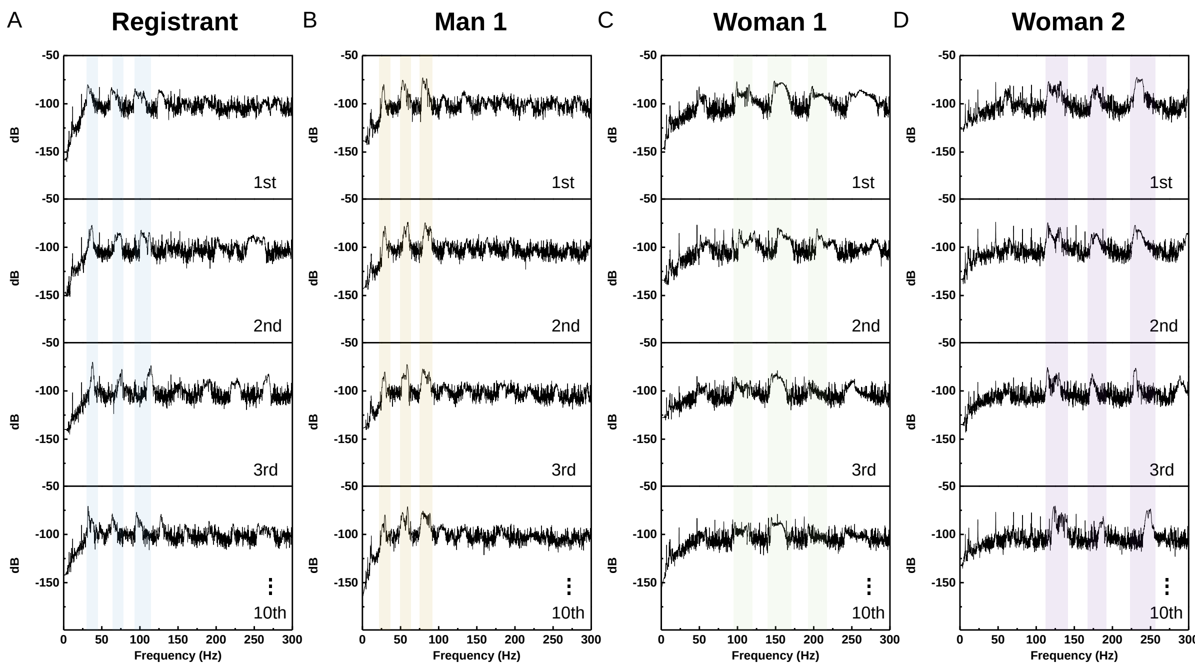

Fig. S20. FFTs for a test repeated 10 times, extracted from the sound wave of the word "hello" obtained from various voices of different subjects including the registrant, a man, and two women.